RSC Advances

PAPER

View Article Online
View Journal | View Issue

Cite this: *RSC Adv.*, 2021, **11**, 3445

Preparation of hybrid paper electrode based on hexagonal boron nitride integrated graphene nanocomposite for free-standing flexible supercapacitors†

Jerome Rajendran,[a] Anatoly N. Reshetilov[b] and Ashok K. Sundramoorthy *[a]

Flexible energy storage devices have received great interest due to the increasing demand for wearable and flexible electronic devices with high-power energy sources. Herein, a novel hybrid flexible hexagonal boron nitride integrated graphene paper (BN/GrP) is fabricated from 2D hexagonal boron nitride (h-BN) nanosheets integrated with graphene sheets dispersion *via* a simple vacuum filtration method. FE-SEM indicated that layered graphene nanosheets tightly confined with h-BN nanosheets. Further, the Raman spectroscopy confirmed successful integration of BN with graphene. As-prepared BN/GrP free-standing flexible conductive paper showed high electrical conductivity of 5.36 × 10^4 S m^{-1} with the sheet resistance of 8.87 Ω sq^{-1}. However, after 1000 continuous bending cycles, the BN/GrP sheet resistance increased just about 8.7% which indicated good flexibility of the paper. Furthermore, as-prepared BN/GrP showed excellent specific capacitance of 321.95 F g^{-1} at current density of 0.5 A g^{-1}. In addition, the power and energy densities were obtained as 3588.3 W kg^{-1}, and 44.7 W h kg^{-1}, respectively. The stability of the prepared flexible electrode was tested in galvanostatic charge/discharge cycles, where the results showed the 96.3% retention even after 6000 cycles. These results exhibited that the proposed BN/GrP may be useful to prepare flexible energy-storage systems.

Received 22nd December 2020
Accepted 6th January 2021

DOI: 10.1039/d0ra10735b

rsc.li/rsc-advances

Introduction

Over the past decade, significant research progress has been made to prepare flexible supercapacitors (SCs) for smart and efficient energy-storage devices because of their remarkable applications in wearable and miniaturized electronic devices.[1,2] So far, majority of the flexible SCs have been fabricated using two dimensional (2D) layered materials such as graphene,[3,4] molybdenum disulfide (MoS_2),[5] hexagonal boron nitride (h-BN),[6] cobalt selenide ($CoSe_2$),[7] tin oxide (SnO_2)[8,9] and tungsten disulfide (WS_2).[10] These 2D layered materials have offered excellent chemical and anisotropic properties due of their interconnected crystalline arrangements.[11–15] Similarly, traditional supercapacitors have also been prepared using carbon-based materials and MoS_2.[16–20] Although, significant research progress has been made with various carbon-based materials, the emphasis on graphene and h-BN nanosheets based hybrid material is growing due to their high thermal conductivity, mechanical strength, optical transparency, flexibility, thermal stability (up to 1000 °C), chemical tolerance (for protective coatings) and so on.[11,14,15,21–30] Therefore, researchers have been exploited these materials in various research fields.

2D-nanosheets (examples: graphene and h-BN) could be used to form various morphologies such as nanotubes and layer-by-layer structures. In recent times, various strategies have been reported to prepare nanosheets by adopting either top-down or bottom-up methods.[31,32] Epitaxial growth and chemical vapour deposition (CVD) are well known bottom-up techniques,[33,34] which suffers from limited scaling up and expensive production cost; nevertheless, it offers high-quality defect-free sheets. Similarly, top-down techniques[35,36] such as mechanical cleavage, electrochemical and liquid phase exfoliation could be utilized to prepare the scalable high-quality defect-free sheets at a much lower cost using bulk h-BN and graphite sheet. Furthermore, these 2D-nanosheets (graphene, h-BN, MoS_2 and WS_2) have been combined to prepare flexible paper,[37] foam[38]

[a]*Department of Chemistry, SRM Institute of Science and Technology, Kattankulathur-603 203, Tamil Nadu, India. E-mail: ashokkus@srmist.edu.in*

[b]*G.K. Skryabin Institute of Biochemistry and Physiology of Microorganisms of the Russian Academy of Sciences (IBPM RAS), Subdivision of "Federal Research Center Pushchino Biological Research Center of the Russian Academy of Sciences" (FRC PBRC RAS), 142290, Pushchino, Moscow oblast, Russia*

† Electronic supplementary information (ESI) available: Schematic illustration for the preparation of freestanding BN/GrP flexible paper using BN/graphene dispersion, preparation of BN/GrP electrode for electrochemical measurements of supercapacitor; EDX mapping analysis of BN/GrP; the peak current was plotted against the scan rate to determine the "*b*" value of the BN/GrP anodic curve; galvanostatic charge/discharge (GCD) curves for GrP and BN/GrP electrodes at a current density of 1 A g^{-1}; comparison of specific capacitances, retention and power density of the reported supercapacitors were provided. See DOI: 10.1039/d0ra10735b

and film[39] through several methods such as mechanical pressuring of 2D-nanosheets aerogels[40,41] or hydrogels,[42] vacuum filtration[3,4] and drying on flexible substrates.[39] As prepared, freestanding 2D-nanosheets based papers had shown great mechanical strength, low density and high electrical conductivity,[43,44] which can be applied in biosensors, actuators, shape memory devices and reliable source of energy storage, such as batteries and supercapacitors (SCs).[36,45] However, there are some vital challenges in developing flexible SCs. For examples, (i) requirement of flexible electrode materials with high efficiency, (ii) enhanced interface performance between electrolytes and electrodes, and (iii) simple device preparation process.[2] So, the development of highly efficient flexible SCs are required as an alternative energy source at low cost. Recently, graphene-based hybrid films have received more attention in developing flexible electrodes. Liu *et al.*,[46] reported rGO film, which had the capacity of 81.7 F g^{-1} at 10 mV s^{-1}. Freeze-drying method[47] was used to prepare graphene paper as an electrode material with the capacity of 172 F g^{-1} at 1 A g^{-1}. Sadak *et al.*,[4] have also used the electrochemical deposition method to prepare GrP/MnO_2 composite with good super-capacitive performance.

In this work, graphene nanosheet dispersion is prepared by electrochemical exfoliation technique which may depends on the intercalation of ions/molecules with graphite layers in an electrolytic cell where graphite sheets are used as electrodes.[48,49] Similarly, the dispersion of h-BN nanosheets is prepared by a liquid phase exfoliation that yielded a significant amount of h-BN nanosheets. Finally, using graphene and h-BN nanosheet co-dispersion, a binary hybrid flexible paper (BN/GrP) is obtained by vacuum filtration (Scheme S1†). Field emission scanning electron microscopy (FE-SEM) and Raman spectroscopy results confirmed that h-BN homogeneously integrated with graphene. Moreover, the BN/GrP paper electrode exhibited high specific capacitance of 321.95 F g^{-1} at 0.5 A g^{-1} current density in 1 M H_2SO_4 and stable charging/discharging cycle stability up to 6000 cycles.

Experimental

Materials

Graphite sheets are obtained from Graphite Shop, Inc. (USA). Hexagonal boron nitride (h-BN) was purchased from Sigma-Aldrich, India. Sodium phosphate dibasic heptahydrate ($Na_2HPO_4 \cdot 7H_2O$) and sodium dihydrogen phosphate monohydrate ($H_2NaPO_4 \cdot H_2O$) were purchased from Spectrochem Pvt, Ltd, India. Potassium chloride (KCl) was purchased from Fisher Scientific, India. All chemicals were used without further any purification. Distilled water (18.2 MΩ cm at room temperature) was collected from a Millipore ultrapure water system.

Characterizations

The microstructure and morphological features of the BN/GrP were characterized by field emission scanning electron microscope (FESEM-EDS) (Quanta 400 FEG, FEI). Raman spectroscopy was performed at ambient condition using LabRAM HR evolution, (Horiba). X-ray diffraction data was acquired (XRD) (X'Pert Powder XRD system, Malvern Panalytical, United Kingdom) with Cu-Kα radiation (λ = 0.15406 nm) at 45 kV (tension) and 40 mA (current) with a 0.02° per step scan at 1° per min speed. Sheet resistance (R_s) was calculated by a two-point probe station (Keithley 2612B, USA) using the following equation,[3]

$$R_s = c_f \frac{V}{I} \quad (1)$$

where, c_f is the correction factor [π/ln(2)], V is the potential and I is the applied current.

An electrochemical workstation CHI-760E (CH Instrument, USA) was used to perform the electrochemical measurements with platinum wire and Ag/AgCl (3 M KCl) as counter and reference electrodes with a three-electrode system. BN/GrP (freestanding film) was used as a working electrode. The galvanostatic charge/discharge (GCD) and cyclic voltammetry (CV) measurements were carried out with 1 M H_2SO_4. The working BN/GrP electrode is fabricated as reported elsewhere.[3,4] Briefly, peeled BN/graphene paper (BN/GrP) was attached to a polyethylene terephthalate (PET) substrate using double-sided carbon tape to allow optimal electrical contact using an alligator clip with a copper tape (Fig. S1†).

The specific capacitance (C_p, F g^{-1}) of our proposed flexible paper was calculated by the following equation, (galvanostatic charge/discharge curves):[50–52]

$$C_p = \frac{I\Delta t}{m\Delta V} \quad (2)$$

where, I is the discharge current (A), m is the mass of the active material on the electrode (g), ΔV is the potential window (V) and Δt is the discharge time (s).

According to the following equations, energy density (E) and power density (P) were determined:[50,53–55]

$$E = \frac{\frac{1}{2}C_p(\Delta V)^2}{3.6} \quad (3)$$

$$P = \frac{E}{t} \times 3600 \quad (4)$$

where, C_p is the specific capacitance (F g^{-1}), ΔV is the potential window (V), and t is the discharge time.

Preparation of h-BN/graphene nanocomposite dispersion

In a typical experiment, the hybrid h-BN/graphene nanosheet dispersion was prepared according to our previously reported procedure.[29] Briefly, 500 mg of h-BN powder was dispersed through bath-sonication in 0.1 M of phosphate-buffer solution (PBS) (pH 7), followed by tip sonication for about 2 h. Further, the above prepared h-BN nanosheets dispersion was centrifuged for 40 min at 4000 rpm. Then, top one third portion was collected and washed with water several times to remove PBS. Then, fresh distilled water was added into BN nanosheets to re-disperse it. This step was repeated 3–4 times to remove all sodium salts and anions from the BN. Finally, h-BN nanosheets

are re-dispersed in distilled water and the concentration of BN was maintained as 3 mg mL^{-1}.

On the other hand, graphene dispersion was synthesized *via* simple electrochemical exfoliation method.[3,4] Initially, the graphite sheets (40 mm × 8 mm) were employed as both cathode and anode electrodes which were placed in 10 mL of 0.1 M PBS (pH 7) and an applied voltage of 10 V was supplied for 30 min. The obtained graphene sheets are collected and washed with water. After that, it was re-dispersed in distilled water using tip sonication. The graphene dispersion was then centrifuged for 40 min at 4000 rpm and the resulted graphene suspension (5 mg mL^{-1}) was collected from the top supernatant (~70%) solution. Furthermore, BN and graphene dispersions were mixed in the ratio of 1 : 9 and continuously stirred for 2 h using a magnetic stirrer at RT, followed by tip sonication for 1 h. The resultant BN/graphene dispersion was utilized for the preparation of flexible paper.

Preparation of BN/graphene paper (BN/GrP)

As illustrated in Scheme S1,† BN/GrP was prepared by a vacuum filtration method. Briefly, 3 mL of BN/graphene (4.5 mg mL^{-1}) dispersion was mixed with 75 mL of water and then 1 M of H_2SO_4 was used to change the pH to ~3.5. After that, BN/graphene dispersion was filtered through cellulose nitrate membrane filter paper (pore size = 0.45 μm) and naturally dried for overnight as shown in Fig. 1a. Finally, it was possible to peel off the BN/GrP from the filter paper (Fig. 1b).

Results and discussion

SEM-EDS analysis

The prepared flexible BN/GrP was mechanically stable and it can be easily bent or/cut into preferred shape as shown in Fig. 1a–f. It is also possible to control the thickness of BN/graphene paper (BN/GrP) by adjusting the concentration and volume of the dispersion. The cross-sectional view of the BN/GrP was recorded by FE-SEM, which showed the thickness of ~21 μm (4.5 mg mL^{-1}). As observed, BN/GrP is made of tightly well stacked and interconnected layered sheets (Fig. 2a and b). In addition, the energy dispersive X-ray spectroscopy (EDS) mapping pattern (Fig. S2†) supported the elementary composition of BN/GrP, which clearly showed the uniformity of boron and nitrogen along with carbon and oxygen presence over the entire BN/GrP region. EDS has also confirmed that B (21.73%), N (26.55%), C (40.02%) and O (11.70%) were present in the respective atomic percentages in the BN/GrP as shown in Fig. S3.†

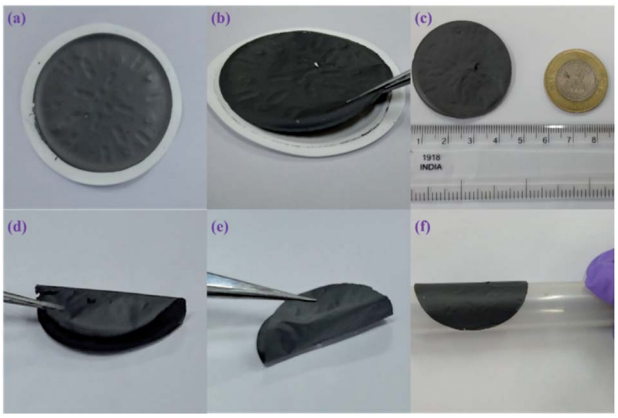

Fig. 1 Visual images of flexible paper of BN/GrP. (a) Room temperature drying, (b) BN/GrP peeled off after drying from the filter paper, (c) BN/GrP freestanding paper, and (d–f) flexibility of BN/GrP.

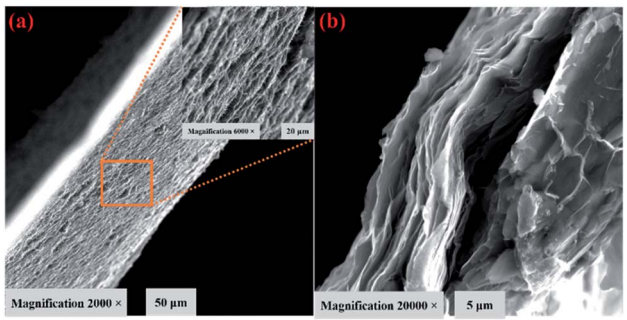

Fig. 2 FE-SEM images of (a) cross sectional views of BN/GrP (inset) at low and (b) high magnifications.

Raman, XRD and electrical measurements

The Raman spectrum of BN/GrP and GrP are shown in Fig. 3a, in which the I_{2D}/I_G ratio of GrP and BN/GrP were less than 0.5, indicated the multilayer structure of the graphene with BN. GrP typically has two distinctive peaks at 1330 and 1581.2 cm^{-1}, respectively, displaying D and G bands.[56] Further, BN/GrP spectrum is exhibited both strong D (~1326.3 cm^{-1}) and G (~1576.6 cm^{-1}) bands which confirmed the presence of graphene. Moreover, strong D band at 1326.3 cm^{-1}, indicated that E_{2g} vibration mode of BN peak which is overlapped with the D band of graphene.[57]

In Fig. 3b, XRD pattern (red curve) of h-BN's revealed a sharp peak at 26.5° due to the (002) plane of h-BN. The weaker peaks at 2θ of 41.5, 54.7 and 75.8° are indexed as (101), (102) and (110) plane's correspond to h-BN (JCPDS file 073-2095).[58] As expected, graphene was showed (blue curve) a broad peak around 24.9°. However, after the intercalation of h-BN with graphene, XRD pattern of the BN/GrP showed (black curve) a broad peak around the 2θ of 25.7° as h-BN. Due to the overlap of the XRD peaks of h-BN with graphene, it was hard to distinguish the peaks. But, the XRD peak at 42.3° indicated the (101) plane of h-BN present in BN/GrP, which confirmed the formation of hybrid paper (BN/GrP).

Next, the sheet resistance and electrical conductivity of the BN/GrP were measured using a two-point probe station (Keithley 2612B, USA) on the flexible hybrid paper in different locations (each measurement was repeated three times). Fig. 3c shows the linear current–voltage (*I–V*) curve of BN/GrP, which indicated the ohmic behaviour of BN/GrP paper. The conductivity and sheet resistance were calculated as 5.36 × 10^4 S m^{-1} and 8.87 Ω sq^{-1}, respectively. Furthermore, the mechanical strength and flexibility of the BN/GrP were tested by measuring

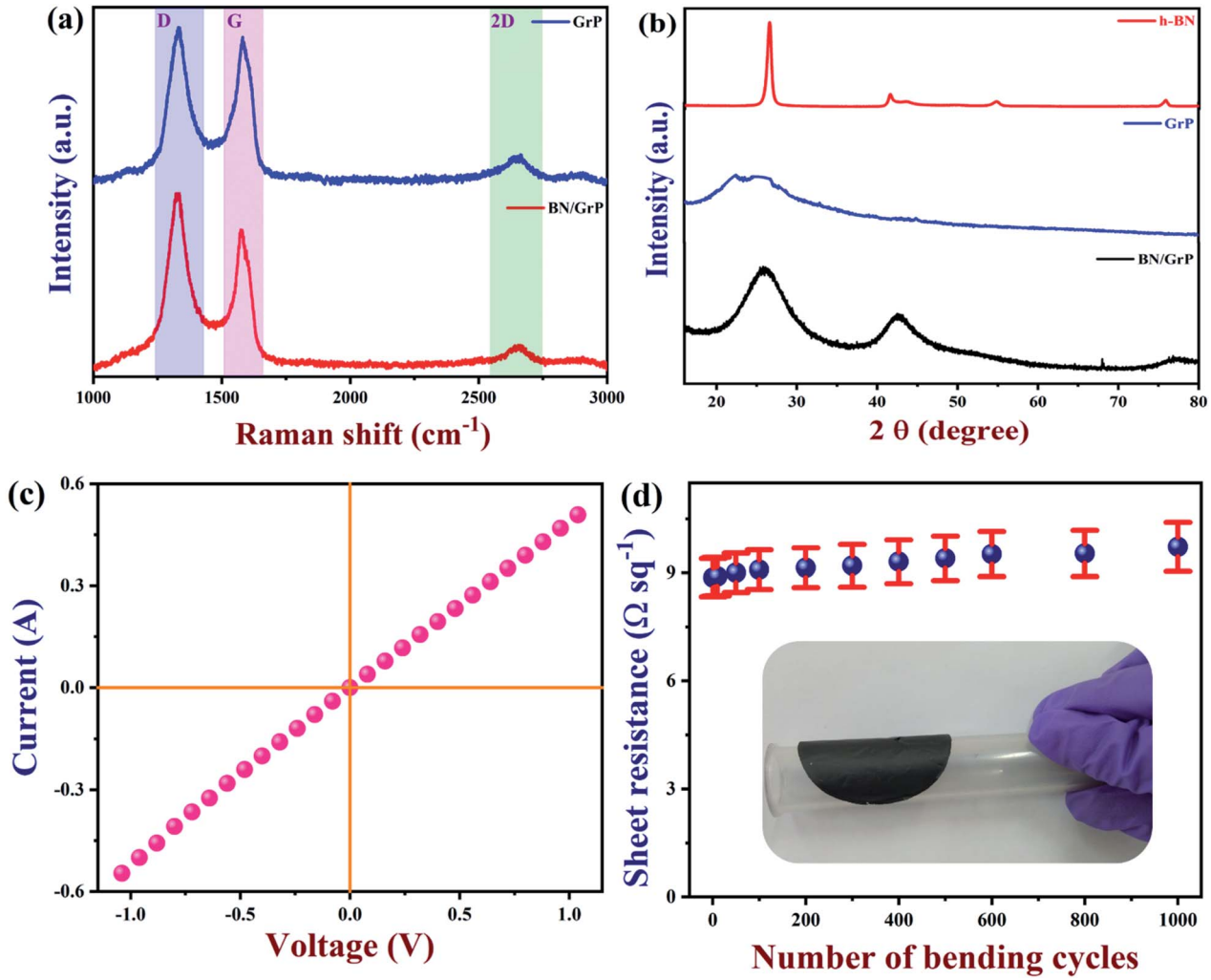

Fig. 3 (a) Raman spectra of BN/GrP and GrP, (b) XRD pattern of h-BN, GrP and BN/GrP (c) current *vs.* voltage response of BN/GrP and (d) flexibility test carried out on BN/GrP (sheet resistance *vs.* number of bending cycles; $n = 3$).

the sheet resistance after bending the paper up to 1000 cycles (at the bending angle of 60°). The sheet resistance was increased about 8.7%. It was again demonstrated that as-prepared BN/GrP had high mechanical stability due to interconnected network of the film (Fig. 3d).

Electrochemical properties of BN/GrP electrode

The electrochemical properties of BN/GrP are evaluated by cyclic voltammetry (CV), galvanostatic charge–discharge (GCD), electrochemical impedance spectroscopy (EIS) and potential cycling test using a three-electrode configuration with 1 M H_2SO_4 as the electrolyte. As shown in Fig. 4a, CV measurements were carried out using BN/GrP at a scan rate of 100 mV s^{-1} in the potential window of 0 to 1.8 V. The rectangular symmetric shape of the CV curves were maintained; even when the potential window was increased up to 1.8 V without any oxygen evaluation peak, which indicated the good capacitive behaviour of BN/GrP. Fig. 4b depicts CV curves of BN/GrP recorded at different scan rates (1 to 100 mV s^{-1}) between 0 and 1 V. Even at a high scan rate of 100 mV s^{-1}, the rectangular shape of CV curve retained without obvious distortion. It might be due to the desirable fast charging/discharging properties and high capacitive behaviour of BN/GrP. In order to ascertain the detailed charge storage behaviour of the BN/GrP, the kinetics process of electrode was examined by using CV measurements. In general, the relationship between the current (i) and scan rate (v) is given by,[5]

$$i = av^b \quad (5)$$

where, 'a' and 'b' are constants; i is the current (mA) and v is the scan rate (mV s^{-1}). The overall current exhibited by the BN/GrP was contributed from diffusion-controlled charge storage and the surface-controlled capacitive processes.[59] In the eqn (5), if the value of $b = 1$, implies capacitive-dominant behaviour, while $b = 0.5$ reflects an electrochemical mechanism dominated by a diffusion process. By fitting the curve against log(i) *vs.* log(v), the value of 'b' can be determined. From the Fig. S4,† 0.64 was determined as 'b' value, which indicated that both capacitive and diffusion-controlled behaviours were observed with the BN/GrP.[5] The GCD curves were strongly symmetrical up to 1.2 V at

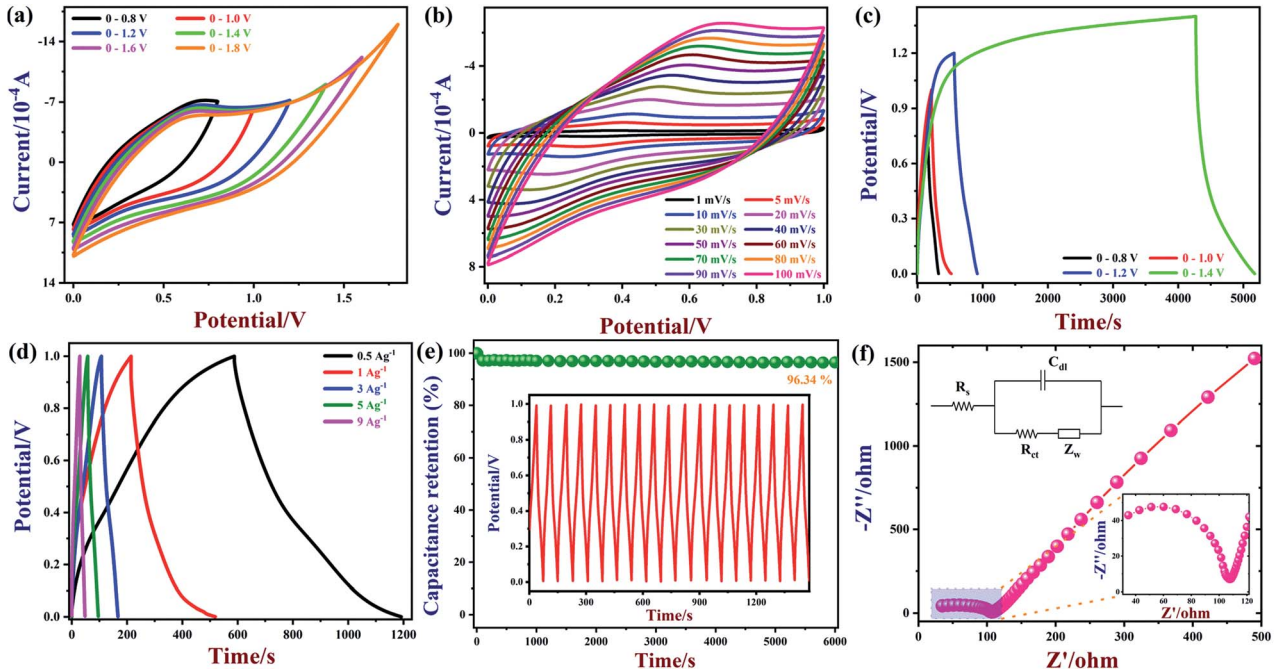

Fig. 4 (a) CVs of BN/GrP at different potential window in 1 M H_2SO_4 (scan rate = 100 mV s^{-1}), (b) CVs of BN/GrP at different scan rates from 1 to 100 mV s^{-1} in 1 M H_2SO_4, (c) GCD curves of BN/GrP with different potential windows at a steady current density of 1 A g^{-1}. (d) GCD curves of BN/GrP at different current density with fixed potential window, (e) cycle life of BN/GrP at constant current density of 4 A g^{-1} (inset: 6000 cycles life of BN/GrP) and (f) Nyquist plot of BN/GrP in 0.1 M KCl containing 5 mM $[Fe(CN)_6]^{3-/4-}$ with frequency range from 0.1 Hz to 1000 kHz (inset: randles equivalent circuit model where, R_s, R_{ct}, C_{dl} and Z_w are solution resistance, charge-transfer (or Faraday) resistance, double layer capacitance and Warburg impedance, respectively).

various potential windows from 0.8 to 1.4 at 1 A g^{-1} as shown in Fig. 4c, which suggested that BN/GrP (flexible paper) had high electrochemical reversibility. Meanwhile, the GCD curves of BN/GrP in the potential window of 0 to 1 V at varying current densities are recorded as shown in Fig. 4d. As can be seen, the charge/discharge curves exhibited an equilateral-triangular shapes which pointed out to a high reversibility without IR drop.

Next, the specific capacitance of the BN/GrP was calculated using GCD curves as 321.95 F g^{-1} at a current density of 0.5 A g^{-1} (Fig. 4d). As noted, the specific capacitance value was decreased with an increasing current density. The energy density (E) and power density (P) of the BN/GrP were calculated and summarized using GCD curves. As prepared BN/GrP exhibited the excellent power density of 44.7 W h kg^{-1} at 0.5 A g^{-1} and high energy density of 249.99 W kg^{-1}. In order to examine the electrochemical properties of the as-synthesized GrP and BN/GrP electrodes, the GCD curves were recorded in 1 M H_2SO_4 in the potential range of 0.0 to 1.0 V at a current density of 1 A g^{-1} (Fig. S5†). Compared with GrP, the BN/GrP electrode was demonstrated longer charging/discharging time as well as high specific capacitance. It may be due to the charge storage capacity of BN/GrP as a function of the free π electrons and the respective changes in the oxidation state of B and N atoms.[60] Furthermore, the cycle life of BN/GrP was tested by repeating the GCD curves between 0 and 1 V at a current density of 4 A g^{-1} up to 6000 cycles (Fig. 4e inset). After 6000 cycles, 93.6% of capacitance was retained as shown in Fig. 4e. Electrochemical impedance spectroscopy (EIS) spectrum of BN/GrP was recorded in 0.1 M KCl electrolyte containing $Fe(CN)_6^{4-/3-}$. The diameter of the semicircle is directly proportional to the charge transfer resistance (R_{ct}).[61] In Fig. 4f, the diameter of semicircle was indicated the high R_{ct} (72.1 Ω) with low equivalent series resistance (R_s ~ 34.75) of BN/GrP. The electrochemical properties of previously reported materials[3,4,46,47,62] were also compared with our proposed BN/GrP in Table. S1.† It was found that BN/GrP had showed higher specific capacitance and good cycling stability compared to some of the reported electrodes.

Conclusions

In summary, the hexagonal boron nitride (h-BN) nanosheets were integrated with graphene to prepare a flexible free-standing paper which showed high electrical conductivity of 5.36×10^4 S m^{-1} and sheet resistance of 8.87 Ω sq^{-1}. Furthermore, Raman spectroscopy and FE-SEM results had confirmed the successful integration of BN within graphene paper. This flexible paper electrode exhibited high specific capacitance of 321.95 F g^{-1} at 0.5 A g^{-1}. It also showed excellent energy density of 44.7 W h kg^{-1} and power density of 3588.3 W kg^{-1} in a three-electrode system. Moreover, the prepared flexible paper showed reasonable stability even after 6000 charging/discharging cycles. From the above results, we believe that our proposed

flexible BN/GrP has high potential to be used as wearable/flexible power sources for the next generation flexible electronics.

Author contributions

AKS and JR both conceived the idea. JR carried out all the experiments. Both AKS and JR interpreted the results and wrote the manuscript. RA provided useful suggestions and supported our research to improve scientific content of the manuscript.

Conflicts of interest

There are no conflicts to declare.

Acknowledgements

We sincerely thank Department of Science and Technology (DST) (International Bilateral Cooperation Division), India for financial support through "INDO-RUSSIA Project (File No. INT/RUS/RFBR/385)". JR thanks SRM IST for PhD student fellowship.

References

1 B. G. Choi, J. Hong, W. H. Hong, P. T. Hammond and H. Park, *ACS Nano*, 2011, **5**, 7205–7213.
2 Z. Wu, A. Winter, L. Chen, Y. Sun, A. Turchanin, X. Feng and K. Müllen, *Adv. Mater.*, 2012, **24**, 5130–5135.
3 O. Sadak, A. K. Sundramoorthy and S. Gunasekaran, *Carbon*, 2018, **138**, 108–117.
4 O. Sadak, W. Wang, J. Guan, A. K. Sundramoorthy and S. Gunasekaran, *ACS Appl. Nano Mater.*, 2019, **2**, 4386–4394.
5 G. Suo, J. Zhang, D. Li, Q. Yu, M. He, L. Feng, X. Hou, Y. Yang, X. Ye, L. Zhang and W. Wang, *J. Colloid Interface Sci.*, 2020, **566**, 427–433.
6 T. Li, X. Jiao, T. You, F. Dai, P. Zhang, F. Yu, L. Hu, L. Ding, L. Zhang, Z. Wen and Y. Wu, *Ceram. Int.*, 2019, **45**, 4283–4289.
7 G. Suo, J. Zhang, D. Li, Q. Yu, W. Wang, M. He, L. Feng, X. Hou, Y. Yang, X. Ye and L. Zhang, *Chem. Eng. J.*, 2020, **388**, 124396.
8 D. Li, J. Zhang, S. M. Ahmed, G. Suo, W. Wang, L. Feng, X. Hou, Y. Yang, X. Ye and L. Zhang, *J. Colloid Interface Sci.*, 2020, **574**, 174–181.
9 G. Suo, D. Li, L. Feng, X. Hou, X. Ye, L. Zhang, Q. Yu, Y. Yang and W. Wang, *J. Mater. Sci. Technol.*, 2020, **55**, 167–172.
10 W. Chen, X. Yu, Z. Zhao, S. Ji and L. Feng, *Electrochim. Acta*, 2019, **298**, 313–320.
11 M. Xu, T. Liang, M. Shi and H. Chen, *Chem. Rev.*, 2013, **113**, 3766–3798.
12 A. Ciesielski and P. Samorì, *Chem. Soc. Rev.*, 2014, **43**, 381–398.
13 Y. Sheng, T. Chen, Y. Lu, R.-J. Chang, S. Sinha and J. H. Warner, *ACS Nano*, 2019, **13**, 4530–4537.
14 M. A. Yamoah, W. Yang, E. Pop and D. Goldhaber-Gordon, *ACS Nano*, 2017, **11**, 9914–9919.
15 R. Jerome and A. K. Sundramoorthy, *J. Electrochem. Soc.*, 2019, **166**, B3017–B3024.
16 D. Wang, Y. Xiao, X. Luo, Z. Wu, Y.-J. Wang and B. Fang, *ACS Sustainable Chem. Eng.*, 2017, **5**, 2509–2515.
17 B. Fang, Y.-Z. Wei, K. Suzuki and M. Kumagai, *Electrochim. Acta*, 2005, **50**, 3616–3621.
18 B. Fang, J. H. Kim, M.-S. Kim and J.-S. Yu, *Acc. Chem. Res.*, 2013, **46**, 1397–1406.
19 B. Fang, A. Bonakdarpour, M.-S. Kim, J. H. Kim, D. P. Wilkinson and J.-S. Yu, *Microporous Mesoporous Mater.*, 2013, **182**, 1–7.
20 B. Fang, Y.-Z. Wei and M. Kumagai, *J. Power Sources*, 2006, **155**, 487–491.
21 X. Yang, M. Xu, W. Qiu, X. Chen, M. Deng, J. Zhang, H. Iwai, E. Watanabe and H. Chen, *J. Mater. Chem.*, 2011, **21**, 8096–8103.
22 Y. Gao, X. Chen, H. Xu, Y. Zou, R. Gu, M. Xu, A. K.-Y. Jen and H. Chen, *Carbon*, 2010, **48**, 4475–4482.
23 K. S. Kim, Y. Zhao, H. Jang, S. Y. Lee, J. M. Kim, K. S. Kim, J.-H. Ahn, P. Kim, J.-Y. Choi and B. H. Hong, *Nature*, 2009, **457**, 706.
24 Y. Zhu, S. Murali, M. D. Stoller, K. J. Ganesh, W. Cai, P. J. Ferreira, A. Pirkle, R. M. Wallace, K. A. Cychosz, M. Thommes, D. Su, E. A. Stach and R. S. Ruoff, *Science*, 2011, **332**, 1537–1541.
25 D. Golberg, Y. Bando, Y. Huang, T. Terao, M. Mitome, C. Tang and C. Zhi, *ACS Nano*, 2010, **4**, 2979–2993.
26 M. Deng, X. Yang, M. Silke, W. Qiu, M. Xu, G. Borghs and H. Chen, *Sens. Actuators, B*, 2011, **158**, 176–184.
27 S. Garaj, W. Hubbard, A. Reina, J. Kong, D. Branton and J. A. Golovchenko, *Nature*, 2010, **467**, 190.
28 R. D. Nagarajan and A. K. Sundramoorthy, *Sens. Actuators, B*, 2019, **301**, 127132.
29 R. Jerome and A. K. Sundramoorthy, *Anal. Chim. Acta*, 2020, **1132**, 110–120.
30 R. Jerome, P. V. Keerthivasan, N. Murugan, N. R. Devi and A. K. Sundramoorthy, *ChemistrySelect*, 2020, **5**, 9111–9118.
31 Y. Hernandez, V. Nicolosi, M. Lotya, F. M. Blighe, Z. Sun, S. De, I. T. McGovern, B. Holland, M. Byrne, Y. K. Gun'Ko, J. J. Boland, P. Niraj, G. Duesberg, S. Krishnamurthy, R. Goodhue, J. Hutchison, V. Scardaci, A. C. Ferrari and J. N. Coleman, *Nat. Nanotechnol.*, 2008, **3**, 563–568.
32 K. R. Paton, E. Varrla, C. Backes, R. J. Smith, U. Khan, A. O'Neill, C. Boland, M. Lotya, O. M. Istrate, P. King, T. Higgins, S. Barwich, P. May, P. Puczkarski, I. Ahmed, M. Moebius, H. Pettersson, E. Long, J. Coelho, S. E. O'Brien, E. K. McGuire, B. M. Sanchez, G. S. Duesberg, N. McEvoy, T. J. Pennycook, C. Downing, A. Crossley, V. Nicolosi and J. N. Coleman, *Nat. Mater.*, 2014, **13**, 624.
33 Y. Wang, L. Li, L. Yan, X. Gu, P. Dai, D. Liu, J. G. Bell, G. Zhao, X. Zhao and K. M. Thomas, *Chem. Mater.*, 2018, **30**, 3048–3059.
34 R. Sakamoto, K. Hoshiko, Q. Liu, T. Yagi, T. Nagayama, S. Kusaka, M. Tsuchiya, Y. Kitagawa, W.-Y. Wong and H. Nishihara, *Nat. Commun.*, 2015, **6**, 6713.

35 H. Ba, L. Truong-Phuoc, C. Pham-Huu, W. Luo, W. Baaziz, T. Romero and I. Janowska, *ACS Omega*, 2017, **2**, 8610–8617.
36 P. Garrigue, M.-H. Delville, C. Labrugère, E. Cloutet, P. J. Kulesza, J. P. Morand and A. Kuhn, *Chem. Mater.*, 2004, **16**, 2984–2986.
37 L. Liu, Z. Niu, L. Zhang, W. Zhou, X. Chen and S. Xie, *Adv. Mater.*, 2014, **26**, 4855–4862.
38 J. Sha, C. Gao, S.-K. Lee, Y. Li, N. Zhao and J. M. Tour, *ACS Nano*, 2016, **10**, 1411–1416.
39 V. Strong, S. Dubin, M. F. El-Kady, A. Lech, Y. Wang, B. H. Weiller and R. B. Kaner, *ACS Nano*, 2012, **6**, 1395–1403.
40 Y. Lv, L. Li, Y. Zhou, M. Yu, J. Wang, J. Liu, J. Zhou, Z. Fan and Z. Shao, *RSC Adv.*, 2017, **7**, 43512–43520.
41 S. M. Jung, D. L. Mafra, C.-T. Lin, H. Y. Jung and J. Kong, *Nanoscale*, 2015, **7**, 4386–4393.
42 H. Li, Y. Tao, X. Zheng, Z. Li, D. Liu, Z. Xu, C. Luo, J. Luo, F. Kang and Q.-H. Yang, *Nanoscale*, 2015, **7**, 18459–18463.
43 Z. Zhang, F. Xiao, L. Qian, J. Xiao, S. Wang and Y. Liu, *Adv. Energy Mater.*, 2014, **4**, 1400064.
44 C. Ji, K. Zhang, L. Li, X. Chen, J. Hu, D. Yan, G. Xiao and X. He, *J. Mater. Chem. A*, 2017, **5**, 11263–11270.
45 N. I. Kovtyukhova, N. Perea-López, M. Terrones and T. E. Mallouk, *ACS Nano*, 2017, **11**, 6746–6754.
46 W. Liu, X. Yan, J. Lang, C. Peng and Q. Xue, *J. Mater. Chem.*, 2012, **22**, 17245–17253.
47 F. Liu, S. Song, D. Xue and H. Zhang, *Adv. Mater.*, 2012, **24**, 1089–1094.
48 J. M. Munuera, J. I. Paredes, M. Enterría, A. Pagán, S. Villar-Rodil, M. F. R. Pereira, J. I. Martins, J. L. Figueiredo, J. L. Cenis, A. Martínez-Alonso and J. M. D. Tascón, *ACS Appl. Mater. Interfaces*, 2017, **9**, 24085–24099.
49 A. K. Sundramoorthy, T. H. Vignesh Kumar and S. Gunasekaran, in *Advanced Nanomaterials*, ed. A. B. T.-G. B. Tiwari, Elsevier, 2018, pp. 267–306.
50 M. F. Iqbal, M. Ul-Hassan, M. N. Ashiq, S. Iqbal, N. Bibi and B. Parveen, *Electrochim. Acta*, 2017, **246**, 1097–1103.
51 X. Liang, G. Long, C. Fu, M. Pang, Y. Xi, J. Li, W. Han, G. Wei and Y. Ji, *Chem. Eng. J.*, 2018, **345**, 186–195.
52 D. M. El-Gendy, N. A. A. Ghany and N. K. Allam, *RSC Adv.*, 2019, **9**, 12555–12566.
53 M. Khairy and S. A. El-Safty, *Sens. Actuators, B*, 2014, **193**, 644–652.
54 R. Li, S. Wang, Z. Huang, F. Lu and H. Taobin, *J. Power Sources*, 2016, **312**, 156–164.
55 J. Ma, S. Tang, J. A. Syed and X. Meng, *RSC Adv.*, 2016, **6**, 82995–83002.
56 S. Stankovich, D. A. Dikin, R. D. Piner, K. A. Kohlhaas, A. Kleinhammes, Y. Jia, Y. Wu, S. T. Nguyen and R. S. Ruoff, *Carbon*, 2007, **45**, 1558–1565.
57 M. Wang, T. Zhang, D. Mao, Y. Yao, X. Zeng, L. Ren, Q. Cai, S. Mateti, L. H. Li, X. Zeng, G. Du, R. Sun, Y. Chen, J.-B. Xu and C.-P. Wong, *ACS Nano*, 2019, **13**, 7402–7409.
58 V. Guerra, C. Wan, V. Degirmenci, J. Sloan, D. Presvytis and T. McNally, *Nanoscale*, 2018, **10**, 19469–19477.
59 A. Teli, S. Beknalkar, S. Pawar, D. Dubal, T. Dongale, D. Patil, P. Patil and J. C. Shin, *Energies*, 2020, **13**, 6124.
60 S. Saha, M. Jana, P. Khanra, P. Samanta, H. Koo, N. C. Murmu and T. Kuila, *ACS Appl. Mater. Interfaces*, 2015, **7**, 14211–14222.
61 B. L. Corso, I. Perez, T. Sheps, P. C. Sims, O. T. Gül and P. G. Collins, *Nano Lett.*, 2014, **14**, 1329–1336.
62 Y. He, W. Chen, X. Li, Z. Zhang, J. Fu, C. Zhao and E. Xie, *ACS Nano*, 2013, **7**, 174–182.